Shallow magma dynamics at open-vent volcanoes tracked by coupled thermal and SO$_2$ observations

Marco Laiolo [a,b,*], Dario Delle Donne [c,d], Diego Coppola [a,b], Marcello Bitetto [c], Corrado Cigolini [a], Massimo Della Schiava [e], Lorenzo Innocenti [e], Giorgio Lacanna [e], Francesco Paolo La Monica [c], Francesco Massimetti [a], Marco Pistolesi [f], Maria Cristina Silengo [e], Alessandro Aiuppa [c], Maurizio Ripepe [e]

[a] Dipartimento di Scienze della Terra, Università di Torino, Via Valperga Caluso, 35 - 10125 Torino (TO), Italy
[b] Centro Interdipartimentale Sui Rischi Naturali in Ambiente Montano e Collinare (NATRISK), Università degli Studi di Torino, Largo Paolo Braccini, 2 - 10045 Grugliasco (TO), Italy
[c] Dipartimento di Scienze della Terra e del Mare, Università di Palermo, Via Archirafi, 22 - 90123 Palermo (PA), Italy
[d] Istituto Nazionale di Geofisica e Vulcanologia, Sez. Di Napoli, Osservatorio Vesuviano, Via Diocleziano, 328 - 80124 Napoli (NA), Italy
[e] Dipartimento di Scienze della Terra, Università di Firenze, Via La Pira, 4 - 50121 Firenze (FI), Italy
[f] Dipartimento di Scienze della Terra, Università di Pisa, Via S. Maria, 53 - 56126 Pisa (PI), Italy

ARTICLE INFO

ABSTRACT

Open-vent volcanic activity is typically sustained by ascent and degassing of shallow magma, in which the rate of magma supply to the upper feeding system largely exceeds the rate of magma eruption. Such unbalance between supplied (input) and erupted (output) magma rates is thought to result from steady, degassing-driven, convective magma overturning in a shallow conduit/feeding dyke. Here, we characterize shallow magma circulation at Stromboli volcano by combining independent observations of heat (Volcanic Radiative Power; via satellite images) and gas (SO$_2$, via UV camera) output in a temporal interval (from August 1, 2018 to April 30, 2020) encompassing the summer 2019 effusive eruption and two paroxysmal explosions (on July 3 and August 28, 2019). We show that, during the phase of ordinary strombolian explosive activity that preceded the 2019 effusive eruption, the average magma input rate (0.1-0.2 m^3/s) exceeds the magma eruption rate (0.001-0.01 m^3/s) by ∼2 orders of magnitude. Conversely, magma input and output rates converge to an average of ∼0.4 m^3/s during the summer 2019 summit effusion, implying an overall suppression of magma recycling back into the feeding system, and hence of excess degassing. We find that, during the effusive eruption, the peak in SO$_2$ emissions lags behind the thermal emission peak by ∼27 days, suggesting that magma output, feeding the lava flow field, initially dominates over magma input in the conduit. We propose that this conduit mass unloading, produced by this initial phase of the effusive eruption, leads to an overall decompression (of up to 30 Pa/s) of the shallow plumbing system, ultimately causing ascent of less-dense, volatile-rich magma batch(es) from depth, enhanced explosive activity, and elevated SO$_2$ fluxes culminating into a paroxysmal explosion on August 28. Our results demonstrate that combined analysis of thermal and SO$_2$ flux time-series paves the way to improved understanding of shallow magmatic system dynamics at open-vent volcanoes, and of the transition from explosive to effusive activity regimes.

© 2022 The Author(s). Published by Elsevier B.V. This is an open access article under the CC BY license (http://creativecommons.org/licenses/by/4.0/).

1. Introduction

Open-vent volcanoes are globally significant emitters of heat and volatiles that, during their persistent regular activity, pro-duce more gas than that explained by simple degassing of erupted magma volumes at surface (Francis et al., 1993; Kazahaya et al., 1994). Such excess degassing requires an efficient magma convection mechanism within the feeding system that allows huge parcels of magma to degas without being erupted (Shinohara, 2008). However, this mild and persistent activity characterizing open-vent volcanism can evolve, at times with no or limited precursory signs, into more intense eruptive phenomena such as opening of lateral eruptive vent(s) (Shreve et al., 2019), lava foun-

tain episodes or violent explosions (e.g. Aiuppa et al., 2021; Calvari et al., 2011; Ripepe et al., 2021) that pose a serious hazard for inhabitants living nearby (see also the Nyiragongo May 22-31, 2021 activity as a dramatic example; Boudoire et al., 2022). The processes that drive these rapid changes in eruptive style are difficult to interpret, as they result from a complex interplay between a variety of factors in the deep and/or shallow plumbing systems (e.g. Calvari et al., 2011; Ripepe et al., 2015; Shreve et al., 2019; Aiuppa et al., 2021).

The persistence of background seismicity, gas and/or thermal emissions (Rose et al., 2013) during regular activity often limits our ability to resolve the small deviations in volcanic behavior that can prelude to eruption onset (Valade et al., 2016). A multiparametric monitoring effort is often key to an effective, near real-time interpretation of volcano network time-series (Ripepe et al., 2005; Phillipson et al., 2013). In this view, a well-established ground- and space-based multiparametric monitoring network makes of Stromboli volcano (Italy) an ideal test site to improve our understanding on open-vent volcanoes (Ripepe et al., 2015; Valade et al., 2016). Stromboli's activity ranges from persistent, mild-explosive activity (here referred as ordinary activity) to less frequent but hazardous effusive eruptions and violent explosions of larger scale (Rosi et al., 2013). In July-August 2019, in particular, an effusive eruption took place, initiated and terminated by two sudden and violent paroxysmal explosions on July 3 and August 28, respectively (Aiuppa et al., 2021; Andronico et al., 2021; Giordano and De Astis, 2021; Ripepe et al., 2021). This sequence of events has represented a real challenge for volcanologist and local civil protection authorities.

Here, we investigate the mechanisms of the 2019 Stromboli's effusive eruption by combining near real-time ground- and space-based measurements of the SO_2 and thermal fluxes, obtained from respectively a permanent UV-camera system (Delle Donne et al., 2017; Aiuppa et al., 2021) and the radiant heat flux (Volcanic Radiative Power, VRP; Coppola et al., 2016) obtained from the Moderate Resolution Imaging Spectroradiometer (MODIS). These independent datasets are used to derive rates of magma input into, and output from, Stromboli's shallow magmatic system in a temporal interval (from August 1, 2018 to April 30, 2020) encompassing the July – August 2019 effusive eruption. We show that the resulting magma input/output budgets are suggestive of a complex dynamics involving pressure charge/discharge mechanism as driver for the 2019 Stromboli's effusive eruption. We conclude that combining SO_2 and thermal records (D'Aleo et al., 2018; Laiolo et al., 2018) allow better understanding of the explosive to effusive transition at open-vent open-conduit volcanoes. Although specifically designed to investigate the mechanisms of the summer 2019 effusive eruption, our results also contribute some novel insights into the drivers of the August 28, 2019 paroxysm.

2. Stromboli volcano: background and 2019 eruptive crisis

Stromboli, the "Lighthouse of the Mediterranean", ranks among the most studied open-vent volcanoes in the world (Allard et al., 1994; Ripepe et al., 2008), and is globally renowned for its regular, millennial, mild-explosive "Strombolian" activity (Rosi et al., 2013). This "ordinary" activity manifests into repetitive, discrete gas outburst ejecting bombs, lapilli and ash, occurring during a regular, continuous degassing and puffing activity (Ripepe et al., 2008). This ordinary activity is, much less frequently, punctuated by more energetic events that include effusive lateral eruption, summit overflows, and/or major/paroxysmal explosions (Rosi et al., 2013).

Ordinary activity is fed by a stable degassing process modulated by steady-state convective overturning of the magmatic column, in which gas-rich magma ascends, degases and crystallizes, and then sinks back down the conduit (Allard et al., 1994; Shinohara, 2008).
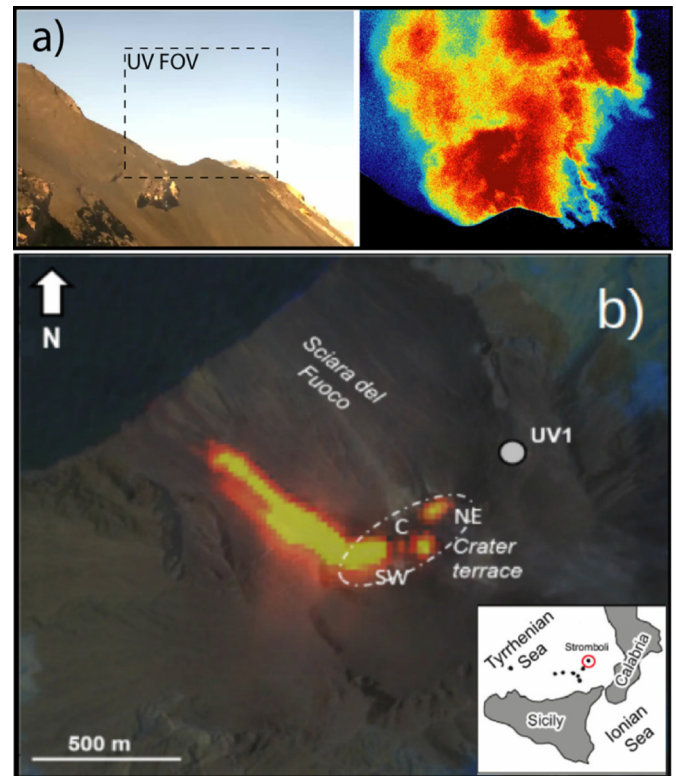

Fig. 1. (a) Example of an SO_2 absorbance image capturing persistent degassing from summit crater area as seen from UV1 permanent UV camera station; camera field of view on the right is also shown by the square in the visible image; (b) satellite image of Stromboli acquired by Sentinel-2 MSI sensor on July 17, 2019 overlapped on a Google Earth® image showing the July-August lava flow field at its maximum extension, and intense thermal irradiance from the Central (C) and North East (NE) craters, produced by strombolian explosive activity.

This mechanism explains why only a small fraction of magma supplying SO_2 degassing at surface is erupted by explosive activity (Allard et al., 1994; Harris and Stevenson, 1997). This magma convection regime is thought to take place within the shallow upper portion of the magmatic column (<3 km depth; Allard et al., 1994; Burton et al., 2009), filled by volatile-poor, High Porphiritic (HP; Francalanci et al., 1999) magma typically erupted during ordinary explosive activity and lava effusions. This HP magma is thought to reside, for 1-60 to 180 years (Petrone et al., 2018; Di Stefano et al., 2020), in a shallow (≤3 km depth) reservoir of 20-90 Mm^3, before being erupted (Bragagni et al., 2014). Paroxysmal explosions occur every ∼5-10 years on average (Rosi et al., 2013), resulting in the eruption of Low-Porphyritic (LP) magma (i.e. golden pumices) during rapid gas/magma ascent from a primitive, gas-rich deep magma reservoir (Aiuppa et al., 2021; Métrich et al., 2010 and reference therein). Paroxysmal explosions, along with lava effusions, pose a real hazard for local villagers, tourists and scientists, considering they can also trigger flank edifice collapses and generate tsunamis (Rosi et al., 2013; Métrich et al., 2021; Ripepe et al., 2021).

The most recent of these "non-ordinary" activity periods occurred in July-August 2019, when Stromboli was hit by a sequence of events that included: (i) a two-months-long effusive eruption from the volcano's summit, and (ii) two paroxysmal explosions (Giordano and De Astis, 2021). Hereafter, we will refer to this complex series of events as the 2019 eruptive crisis. The 2019 eruptive crisis started suddenly on July 3, 2019, at 14.45 UTC, with the strongest ever recorded paroxysmal explosion of the instrumental era (Ripepe et al., 2021). Within a few minutes, partial collapse of a ∼8.4 km-high eruptive column (Giordano and De Astis, 2021)

triggered a pyroclastic flow that, descending along the Sciara del Fuoco, generated a small (few cm) tsunami wave (Lacanna and Ripepe, 2020). The explosions caused partial failure of the central-southwest (C and SW) crater's outer rim, leading to conduit lava overspilling into the southern Sciara del Fuoco slope (Fig. 1). The nearly continuous effusive activity that resulted, sustained by a main effusive vent located in the SW sector of the crater terrace, was accompanied by vigorous explosive activity at the summit craters. The effusive eruption (the main target of this study) lasted until 1 September 2019, three days after a second (slightly less intense) paroxysm that occurred on August 28, 2019 at 10:17 UTC (Ripepe et al., 2021), and that also generated a tsunamigenic pyroclastic flow (Lacanna and Ripepe, 2020).

During its historical activity, Stromboli has been regularly affected by monthly-long effusive episodes during which intense explosions have occurred, and by isolated paroxysmal events not connected to effusive phases (Ripepe et al., 2017; Métrich et al., 2021 and reference therein). The 2002-2003, 2007 and 2014 effusive eruptions were all preceded by a manifest escalation in ordinary explosive activity, occasionally associated with lava overflows, that culminated with the opening of the lateral effusive vents inside the Sciara del Fuoco (Ripepe et al., 2017). Moreover, the 2002-2003 and 2007 effusions were punctuated by paroxysmal explosions during ongoing effusion, which respectively occurred 98 and 16 days after effusion onset (Calvari et al., 2011; Ripepe et al., 2017; Métrich et al., 2021). The 2019 eruptive crisis, therefore, differs from the previous eruptive phases in the following aspects: i) lava outpouring in 2019 was directly initiated by failure of the crater caused by a paroxysmal explosion (July 3, 2019); ii) no pre-effusion escalation in ordinary activity was observed in 2019 (in contrast, the driver of the 2002-2003, 2007 and 2014 effusions was an enhancing shallow magma transport and the ensuing intensification of ordinary strombolian activity; Ripepe et al., 2017); iii) the 2019 effusion directly took place from the summit SW crater (and not farther down inside the Sciara del Fuoco scar), and was accompanied by explosive activity that persisted at sustained levels during the entire effusive period, implying no significant drop of the magmatic column (in contrast, the magma level dropped down in the conduit by hundreds of meters during the previous effusive events; Ripepe et al., 2017); iv) a second paroxysmal explosions hit, only 59 days after the July 3 blast.

3. Dataset and methods

We present results acquired between 1 August 2018 and 30 April 2020 (21 months) by using a permanent, fully automated Ultra-Violet (UV) camera and by Moderate Resolution Imaging Spectroradiometer (MODIS) images. Here, we summarize the methods and analytical procedures used to (i) retrieve the radiant heat power (VRP, in Watt) and the SO_2 flux (td^{-1}), and (ii) to convert them into magma rates and volumes. The complete datasets and limits and uncertainties of the proposed approach are attached and described in the Supplementary Information.

3.1. Volcanic Radiative Power (VRP)

In order to quantify the Volcanic Radiative Power (VRP, in Watt) at Stromboli, we use images acquired by MODIS sensors mounted on board of Terra and Aqua NASA's satellites, launched in February 2000 and May 2002 respectively. With their polar orbits, these satellites are able to acquire about 4 images per day (2 nighttime and 2 daytime). The MODIS Level 1B data (1 km^2 of resolution in the infrared bands) provided by LANCE-MODIS system (http://lance-modis.eosdis.nasa.gov/) is ingested in near real-time into the MIROVA system that outputs, among others, the VRP according

to the MIR-method (Coppola et al., 2016). This methodology provides reliable estimates ($\pm30\%$; Coppola et al., 2016 and reference therein) of heat flux radiated by active lava flows and/or by any hot source having temperature higher than $\sim300°C$. At Stromboli, the analysis of a fifteen years-long dataset allowed to distinguish thermal activity regimes likely associated to activity spanning from mild-explosive to effusive (Fig. 2a; Coppola et al., 2016). Within the August 2018 - April 2020 period, 635 out of the 2834 acquired images ($\sim22\%$) exhibited thermal anomalies related to Stromboli's volcanic activity. In the July – August period, in order to obtain a more robust characterization of the effusive eruption, a one-by-one visual inspection of each alerted images was conducted, to discard those affected by important cloud coverage and/or by unfavorable satellite geometry acquisitions (cf. Coppola et al., 2013, 2016). Consequently, the here reported MODIS dataset consists of 513 alerted images; guarantying an overall heat flux estimates on weekly (about 4 detections per week on average) and daily (about 1.7 detection per day, on average) scale, respectively during ordinary and effusive activity.

3.2. UV camera-derived SO_2 fluxes: measurement principles and associated errors

SO_2 fluxes are obtained from a permanent, fully automated UV camera system installed in May 2014 on the volcano summit, at about ~500 m distance from the active craters (UV1; Fig. 1). Measurement principles of the UV (or SO_2) camera, hardware, software and acquisition/processing routines are described in detail in previous research (see Delle Donne et al., 2017 and reference therein). Our UV camera system is designed to automatically acquire and process sets of images, sampled at 0.5 Hz rate during 6 hour-long daily acquisition cycles (Delle Donne et al., 2017), and has been in operation nearly continuously since June 2014 (the unit is still operational by the time of writing). The UV camera has allowed capturing short and long-term degassing fluctuations associated with changing volcanic intensity through years, particularly those related to the escalation in degassing and explosive activity that preceded the 2014 flank eruption (Delle Donne et al., 2017). Time-series analysis has allowed identifying SO_2 thresholds discriminating between normal and enhanced degassing activity regimes (Fig. 2b), such information being reported on a daily basis in the University of Florence bulletins and reports (LGS Report; http://lgs.geo.unifi.it/) for the Italian Dipartimento Nazionale della Protezione Civile (DPC).

3.3. Magma input and output rates from SO_2 fluxes and MODIS results

3.3.1. SO_2-derived magma input rate

A commonly accepted paradigm is that Stromboli's long-lived behavior is driven by shallow magma convection, in which degassed, non-erupted magma (on the order of 10^6 m^{3}y^{-1}) is recycled back into the volcanic feeding system (Allard et al., 1994; Harris and Stevenson, 1997). A corollary of this mechanism is that, during "ordinary" Strombolian activity, the rate of magma supply (Q_{in}) must be far larger than the mass eruption rate (Q_{out}) ejected from the active craters. Our aim here is to characterize the Stromboli's Q_{in}/Q_{out} shallow magma budget ($\leq$ 3 km depth. e.g. Ripepe et al., 2005; Burton et al., 2009; Aiuppa et al., 2018; Coppola et al., 2019) of the 2019 unrest.

Calculation of the magma supply (Q_{in}) from the so-called "petrologic method" (Devine et al., 1984) is based upon scaling the SO_2 flux released at the vent(s) to the magma sulfur yield, as inferred from the difference between initial (in the undegassed parental magma; as measured in melt inclusions) and final (upon magma eruption; as inferred from groundmass analysis) dissolved
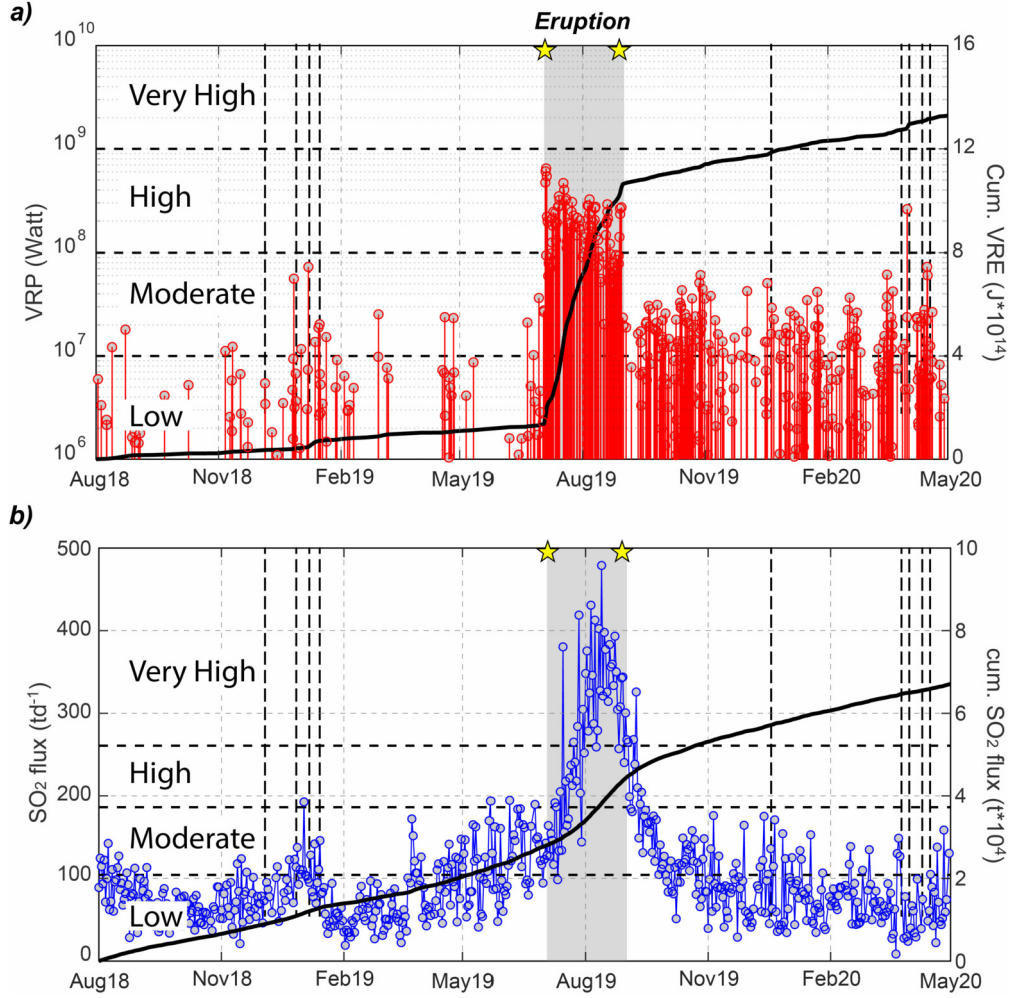
Fig. 2. (a) Volcanic Radiative Power (VRP), in logarithmic scale, and (b) SO$_2$ flux, in linear scale, from August 2018 to May 2020 in relation with the activity thresholds, retrieved by ten-years and five-years long databases, as represented by the horizontal dotted lines (Coppola et al., 2016; LGS Report), together with their associated cumulative thermal energy (Volcanic Radiant Energy; VRE in Joule) and SO$_2$ masses emitted (in tons). Yellow stars indicate the two paroxysmal explosions; grey field represents the effusive period and the dashed lines marked episodic overflows and/or spattering activity as reported by periodic bulletin (see text for details). (For interpretation of the colors in the figure(s), the reader is referred to the web version of this article.)

melt S contents (Allard et al., 1994; Shinohara, 2008). This approach circumvents complexities in S degassing behavior deriving from the large compositional and redox dependencies of sulfur solubility, and from the poorly constrained gas-melt S partition coefficients (Oppenheimer et al., 2018 and reference therein) and it has successfully been used to investigate the S budget of large effusive (Kern et al., 2020) and explosive eruptions (Devine et al., 1984), of continuous degassing associated with lava lakes (e.g. Masaya; Aiuppa et al., 2018), of persistent explosive and effusive activities at open-vent (Allard et al., 1994; Coppola et al., 2019).

The methodology stands on converting the measured surface (plume) SO$_2$ flux (FSO$_2$, in kg/s) into magma input rate (Q$_{in}$) by using equation (Eq. (1)):

$$Q_{in} = \frac{FSO_2}{2 * \Delta XS * \rho_m} \qquad (1)$$

where ρ_m is melt density of the gas-rich magma entering in the shallow system (2500 kg/m^3; Métrich et al., 2010 and reference therein; Ripepe et al., 2021) and ΔXS is the S volatile loss, derived from the difference between parental melt volatile content (from undegassed melt inclusions; 2000 ppm S at Stromboli; Métrich et al., 2010) and the residual S content in the groundmass (200-400 ppm at Stromboli; Métrich et al., 2010). This latter term takes into account the typical crystal fraction of the LP and HP magma

(0.1 and 0.30-0.6, respectively; Stevenson and Blake, 1998; Métrich et al., 2010; Di Stefano et al., 2020). Overall, this relation allows retrieval of the rates of magma degassing and circulation above the SO$_2$ exsolution level (typically at ∼3 km depth at Stromboli). This magma input Q$_{in}$ supplies the shallow convective magma circulation within the conduit (e.g. Allard et al., 1994).

3.3.2. VRP-derived magma output rate

The correlation between thermal flux, active flow area, and lava effusion rates is established by several works (Coppola et al., 2013, 2016 and reference therein). Here we use the so-called radiant approach, which considers a single radiant density term (c_{rad}; in J/m^3) to relate lava discharge rate and thermal radiation for any given rheological case, with an overall error of ± 50% (Coppola et al., 2013). Previous works (Valade et al., 2016; Ripepe et al., 2017) demonstrate the effectiveness, during Stromboli effusive eruptions, of the MODIS-derived Volcanic Radiative Power (VRP) conversion into magma output rate (i.e. TADR), using the equation (Eq. (2)):

$$Q_{out} = \frac{VRP}{c_{rad}} \frac{\rho_{lava}}{\rho_{bulk}} \qquad (2)$$

where ρ_{lava} and ρ_{bulk} are densities of erupted materials and bulk lavas, respectively. Here, we set a ρ_{lava} value of 1850 kg/m^3 as

representative of the overall erupted materials by considering an average bulk lava density of 2000 kg/m^3 (Burton et al., 2009) and the concurrent emission of HP scorias ejected via explosive activity, with density spanning from 900 to 1500 kg/m^3 (Giordano and De Astis, 2021). A c$_{rad}$ coefficient of 2.5*10^8 to 3.75*10^8 J/m^3 has been used previously (Ripepe et al., 2017) to retrieve lava volumes for major effusive phases. For non-effusive, mildly explosive phases, thermal radiance includes contribution from radiation, convection, conduction and ejection of volcanic tephra (e.g. Harris and Stevenson, 1997). Within this framework, we assume that the VRP measured during ordinary activity corresponds to the rate at which magma reaches a depth shallow enough to produce detectable thermal emissions, before being erupted as lapilli or bombs during explosive events (Aiuppa et al., 2018).

3.3.3. Uncertainties of the petrologic method (Q$_{in}$ via SO$_2$ flux) and radiant approach (Q$_{out}$ via volcanic radiative power)

Conversion from SO$_2$ fluxes and VRP into magma input and output rates requires independent knowledge of parameters in equations (1) and (2). These are not fully constrained, and their relative changes can affect dramatically our estimated magma volumes. To quantify/minimize the intrinsic uncertainties of the method, we performed a sensitivity analysis that considers the entire uncertainty ranges of the input parameters. To this aim, from any daily averaged SO$_2$ flux and VRP measurement, we calculate a set of magma input and output rates derived from any possible combination of the petro-physical parameters in eq. (1) and (2). From these, we next calculate the median (50%), and 25-75% quartile distribution boundaries, in order to constrain the intrinsic error associated with the conversion. In particular, for the magma input rate (Q$_{in}$) calculation, we considered the experimental SO$_2$ flux measurement error of ±30%, the residual S content within the groundmass ranging between 200 and 400 ppm, and the crystal fraction of the erupted materials, ranging between 0.45 and 0.6. For the magma output rate calculation, we considered a range of c$_{rad}$ between 2.5*10^8 and 3.75*10^8 J/m^3 (Coppola et al., 2013) and a bulk density (ρ_{bulk}) range between 2500 to 2800 kg/m3 (Cigolini et al., 2015; Ripepe et al., 2015). Due to moderate resolution of the MODIS sensor images (1 km pixel size), we remind that the low-moderate Stromboli summit activity represent a challenge for satellite-based measures (Coppola et al., 2016) thus producing possible large errors on Q$_{out}$ calculation. Applying the method described here, we obtained the magma input and output rate values and their 25% to 75% confidence errors (Figure S1). Combinations between input and output rates are made using their associated

minimum and maximum bounds together with their median values.

4. Results

4.1. VRP and SO$_2$ flux time-series

Our observations, encompassing a 21 months period centered on the 2019 July-August eruption, highlight a distinct temporal evolution for thermal (VRP) and degassing (SO$_2$) activity (Fig. 2).

The ~10 months preceding the summer 2019 eruption are characterized by ordinary Strombolian activity, occasionally punctuated by brief (weeks) periods of increased spattering activity and/or small-volume summit overflows (Fig. 2), as recurrently observed during the latter decade(s) (Coppola et al., 2016). This ordinary activity regime corresponds to relatively steady and low-to-moderate VRP values (typically from 1 MW to 30 MW), with occasional short-lived episodes of VRP increase (to up to 70 MW) that correspond to overflows and/or spattering activity (December 2018 and January 2019; Fig. 2a; INGV Report; LGS Report). During the same period, the SO$_2$ flux (Fig. 2b) remains at generally low levels (average of ~77 t/d), with transient increases up to 200 t/d matching the VRP peaks (Fig. 2a). Since May 2019, the SO$_2$ flux exhibits a mild intensification to "moderate" values of 90 t/d to 180 t/d (Fig. 2b) accompanied by thermal signal which record sporadic VRP peaks up to 20 MW (Fig. 2a).

The July 3 paroxysmal explosion marks the onset of the 2019 eruption, and is thermally tracked by a sudden VRP increase to ~640 MW on July 4, likely due to rapid partial conduit magma drainage into the developing lava flow field, in turn caused by partial crater rim failure during the explosion (Fig. 2, 3). This first VRP peak is short-lived, and is followed by fluctuating thermal anomalies (60-125 MW; Fig. 3) during intermittent effusive activity from 5 to 8 July (LGS Report). Starting from July 9, the VRP increases peaking at 470 MW on July 17 (Fig. 3), and reflecting the emplacement of a ~30,000 m^2 lava field in the upper sector of the Sciara del Fuoco, fed by a lava outpouring from the base of the SW crater (Fig. 1b; Plank et al., 2019). From July 18 onward, the VRP exhibits a waning trend, mimicking an overall decrease of lava effusion until the end of the eruption (September 1), but punctuated by thermal pulses (Fig. 3) likely related to cycles of charge and discharge of lava from the shallow conduit.

The SO$_2$ flux (Figs. 2 and 3) exhibits a contrasting trend (relative to VRP), and gradually increases from July 3 (~150 t/d) to early August, when the "very high" threshold activity level is reached (LGS Report; Fig. 2). After peaking on August 13 (480 t/d),
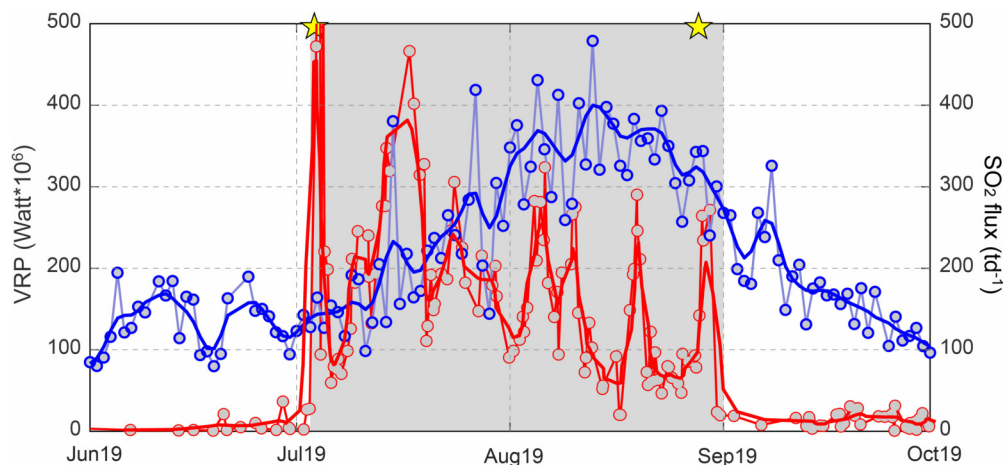

Fig. 3. Close-up of the July-September 2019 eruption period, with lines representing a 7-data points moving average for Volcanic Radiative Power (VRP) and SO$_2$ flux (expressed in linear scale). See Fig. 2 for other symbols.
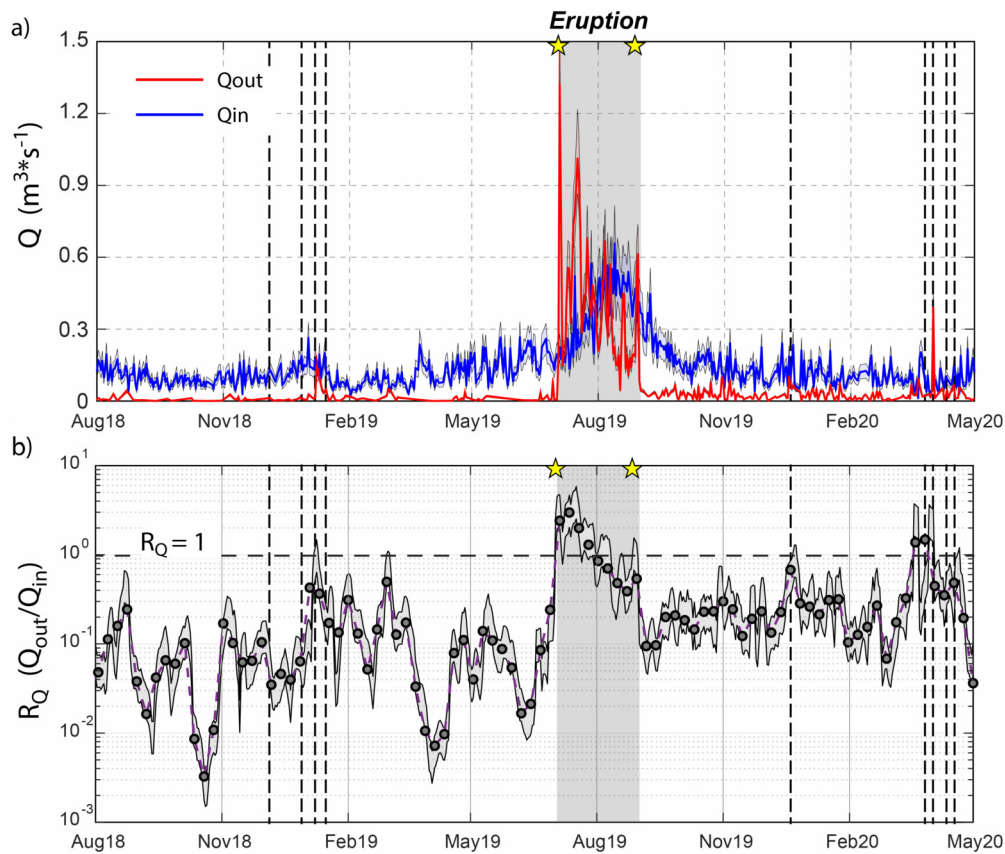
Fig. 4. (a) Daily average of Q_{in} (magma input rate; blue squares) and Q_{out} (magma output rate; red dots), from August 1, 2018 to April 30, 2020 (21 months) obtained by SO_2 and Volcanic Radiative Power dataset; (b) 7-days window average of R_Q ratio (Q_{out}/Q_{in}) respectively retrieved by VRP and SO_2 flux acquired during the Aug. 2018 – Apr. 2020. Grey field represents the daily trend considering the uncertainties as calculated in the method section. See Fig. 2 for other symbols.

circa 40 days after the eruption onset, the SO_2 flux then decreases until the end on the eruption (Fig. 3). It is worth noting that the second paroxysmal explosion occurs on August 28, when both thermal and SO_2 fluxes are still high but showing a general decreasing trend (Fig. 3).

Cessation of effusive activity on September 1 is consistently marked by VRP dropping below 100 MW that is the thermal threshold typically marking the ordinary-to-effusive transition at Stromboli volcano (Coppola et al., 2016). In the post-effusive phase, the persistent of moderate VRP levels (Fig. 2a), and the relatively high (~30%) detection frequency of thermal anomalies, concur to indicate relatively high frequency of strombolian explosions (LGS Report) or, at least, shallow magma circulation in the upper conduits (Coppola et al., 2016). In parallel, the SO_2 flux continues to slowly decline, with background (low) levels being restored in early November (Fig. 2b).

We estimate that, in the 21 months-long analyzed period, the total thermal energy emission is ~$1.3*10^{15}$ J, and the cumulative SO_2 release is ~67 ktons (Fig. 2a, b). More than 70% of the heat (~$0.9*10^{15}$ J), but only 25% of total SO_2 emissions (17 ktons), are released during the 60 days of the eruption, at average rates of 175 MW and 280 t/d, respectively.

4.2. Magma input and output rates

In the pre-eruptive phase (August 2018 – July 2, 2019), our calculated (eq. (1)) Q_{in} is systematically higher (0.1 to 0.3 m^3/s) than Q_{out} (eq. (2)) (Fig. 4a). The latter averages at ~0.003 m^3/s and reaches (or slightly exceeds) 0.1 m^3/s only during the short-lived lava overflows (e.g., January 2019; INGV Report; LGS Report). These estimated Q_{in} and Q_{out} values for ordinary activity match

those previously obtained (Allard et al., 1994; Harris and Stevenson, 1997; Ripepe et al., 2005). In contrast, during the July 3 - August 31, 2019 eruption (Fig. 4a), both Q_{in} and Q_{out} markedly increase, and range 0.12-0.65 and 0.05-1.35 m^3/s, respectively. Q_{out} exceeds Q_{in} during the initial phase of the effusive activity, but this condition is reversed ($Q_{out} < Q_{in}$) since August 2019 (Fig. 4a).

We use the R_Q parameter ($R_Q = Q_{out}/Q_{in}$; Fig. 4b) to characterize the magma input/output relationship more effectively, and to identify distinct thermal/degassing behaviors at Stromboli.

R_Q ranges between 0.1 and 0.01 during ordinary activity (i.e., before July 3, 2019; Fig. 4b), confirming only a small fraction (<10%) of magma supplied to the shallow conduits (and degassing) is eventually erupted via typical Strombolian activity. In contrast, during the 2019 effusive phase, R_Q ratio increases to ~1 or more (Fig. 4b), suggesting a major change in shallow magma dynamic within the conduit.

The contrasting ordinary ($R_Q \sim 0.1$) vs. effusive ($R_Q \sim 1$) magma dynamics are illustrated in Fig. 5. Q_{out} increases by about three orders of magnitude from ordinary to effusive activity, while Q_{in} increases by less than one order of magnitude among the two regimes. An increase of Q_{in} during the 2019 magma effusion at Stromboli is consistent with the dynamics already observed during the 2014 lava flow at Stromboli (Delle Donne et al., 2017), but the SO_2-VRP comparison further allows to evaluate the amount of magma actually recycled and stored back within the shallow magma reservoir.

4.3. Supplied vs. erupted magma volumes

We quantify the total magma volumes involved during the observational period (Fig. 6) by cumulating the volumetric magma in-
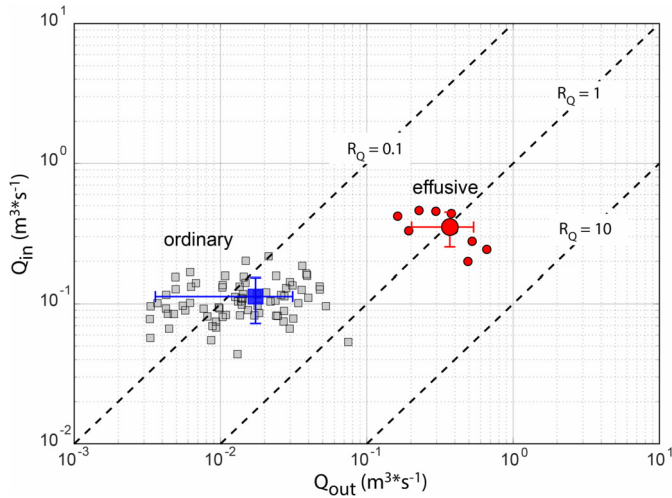
Fig. 5. 7-days window average of Q_{out} vs. Q_{in} obtained on the August 2018 – April 2020 period. Blue squares and red circles represent the overall mean value with their relative error bars of 1σ deviation, for ordinary and eruptive regimes. Black dotted curves represent the Q_{out}/Q_{in} ratios of 0.1, 1 and 10.

put/output rates (Fig. 4). We show that about 8.0 Mm^3 ($\pm$1.2 Mm^3; Fig. 6a) of magma have degassed (at a mean input rate of 0.14$\pm$0.02 m^3/s) during the 21 months-long investigated period; during the same interval, only about 2.7$\pm$0.3 Mm^3 of magma have been erupted (at a mean rate of 0.05$\pm$0.01 m^3/s) (all volumes quoted here are as Dense Rock Equivalent, DRE; see Method section). We additionally calculate that, during the ordinary activity regime, about 0.8 Mm^3 ($\sim$14%) of the 5.6 Mm^3 degassed magma is erupted (the average rates are of ca. 0.015 m^3/s and 0.11 m^3/s). In contrast, during the effusive eruption, the cumulative trends accelerate relative to the ordinary regime (Fig. 6a), and the total input and output magma volumes are roughly equivalent (Vol$_{in}$, 1.95$\pm$0.3 Mm^3; Vol$_{out}$, 2.05$\pm$0.25 Mm^3), further demonstrating a deviation from equilibrium condition. Our derived erupted lava volume (2.05$\pm$0.25 Mm^3) is significantly lower than that obtained by means of space-based thermal measurements (6.3 $\pm$ 3.17 Mm^3; Plank et al., 2019), but agrees well with those obtained by topographic-based methods (1.5 Mm^3 - 2.1 Mm^3; Di Traglia et al., 2021a and reference therein). The discrepancy between our estimate and that of Plank et al. (2019) reflects a combination of (i) a different image database used (see Method section) and (ii) a different c_{rad} value adopted, leading to a large uncertainty (50%) in the volume retrieved by Plank and coauthors, and (iii) the fact that our estimates are expressed in terms of dense rock equivalent.

In order to focus on magma dynamics associated with the effusive eruption, we subtracted the time-averaged ordinary trend (i.e. the amount of magma supplied to, and erupted from the shallow reservoir during ordinary Strombolian activity) from the cumulative Vol$_{in}$ and Vol$_{out}$ curves, and calculate the residual (excess) input and output magma volumes (Fig. 6b). The excess magma input volume (excess Vol$_{in}$) exhibits a moderate, $\sim$1 month-long acceleration prior to the effusion onset that is not associated with any concurrent excess Vol$_{out}$ increase (Fig. 6b). More importantly, the eruption onset marks an abrupt change-in-the-slopes in the excess Vol$_{in}$ and Vol$_{out}$ curves (Fig. 6b) that reflects an anomalously fast magma transport, especially in the first two weeks of the eruption (during which $\sim$1$\pm$ 0.2 Mm^3 of lava were discharged). Notably, the Vol$_{in}$ and Vol$_{out}$ curves exhibit different evolutionary trends during the eruption, but converge at the end of the eruption, when the cumulative excess Vol$_{in}$ and Vol$_{out}$ balance out (Fig. 6b).

5. Discussion

5.1. Modeling magma dynamics within Stromboli's shallow reservoir

Steady-state magma convection in the conduit is thought to drive the long-lasting persistent mild explosive activity at Stromboli, and is the cause for the observed excess degassing (Allard et al., 1994; Harris and Stevenson, 1997). Long-term GPS measurements (Bonaccorso et al., 2009) and satellite InSAR observations (Di Traglia et al., 2021b) point against any long-term deformation of the volcano edifice, suggesting that magma convection does not cause significant volume changes in the Stromboli's plumbing system over decadal timescales (Bonaccorso et al., 2009; Di Traglia et al., 2021b; Mattia et al., 2021).

In the magma convection hypothesis, mass conservation requires magma input (Q_{in}) and output (Q_{out}) rates to be linked by the following equation:

$$Q_{\text{in}} = Q_{out} + Q_D \tag{3}$$

where Q_D is the descending degassed magma flux (recycled back into the conduit). We derive the descending magma flux as the net difference between input (Q_{in}) and output (Q_{out}) magma fluxes ($Q_D = Q_{in} - Q_{out}$, see Fig. 4a).

Results highlight a stable Q_D ($\sim$0.1$\pm$0.02 m^3/s; here referred as Q_D^{ORD}) during ordinary activity, when $Q_D \sim Q_{in}$ implies a high recycling efficiency of the convective column (i.e., 90% of the degassed magma is recycled back into the conduit and not erupted; Fig. 7), in agreement with earlier observations (Allard et al., 1994; Francis et al., 1993; Harris and Stevenson, 1997). A similar degassing regime has been proposed to explain excess S emissions at many other volcanic systems of mafic (e.g., Manam and Etna) to intermediate/silicic (e.g., Bagana and Santiaguito) compositions, at lava lakes (e.g., Masaya), and at volcanoes that exhibit mildly explosive (e.g., Yasur) or lava dome building activity (e.g., Popocatépetl) (see Shinohara, 2008; Edmonds et al., 2022 and reference therein).

In contrast, Q_D strongly deviates from the stable long-term behavior during the 2019 effusive eruption (Fig. 7), with $Q_D << 0$ in the initial phase of the eruption, indicating more magma is erupting than being supplied to the feeding system. Then, during the second half of the effusive eruption, $Q_D > Q_D^{ORD}$, implying heightened magma circulation and recycling efficiency relative to ordinary activity. The occurrence of $Q_D <= 0$ conditions (i.e., effusive phases) implies the magma convection mechanism is temporary suppressed, as already observed at other open-vent systems (e.g., Ambrym and Etna) during lateral effusions or short-lived lava fountaining activity (D'Aleo et al., 2018; Coppola et al., 2019; Shreve et al., 2019). Notably, the 2007 and 2014 Stromboli's effusive phases, erupting about 9.5 Mm^3 and 5.5 Mm^3 (Ripepe et al., 2017), rapidly drained from the shallow conduit by lateral vents. The subsequent replenishment of the shallow conduit (Cigolini et al., 2015; Ripepe et al., 2017) was also accompanied, with complex timing, by similar magma dynamics (e.g. Burton et al., 2009; Cigolini et al., 2015; Delle Donne et al., 2017).

The overall *long-term* stability of Q_D (Fig. 7) during ordinary activity reflects the efficiency of the convective column in recycling degassed magma back into the conduit, while replacing it with an equivalent amount of undegassed magma. This process is not associated by any significant volume and pressure change within the conduit, as evidenced by the lack of long-term deformation (Bonaccorso et al., 2009; Di Traglia et al., 2021a,b). Convection efficiency is controlled by conduit radius and viscosity of descending magma (Stevenson and Blake, 1998), which are unlikely to vary over timescales of a few days. We therefore argue that any change
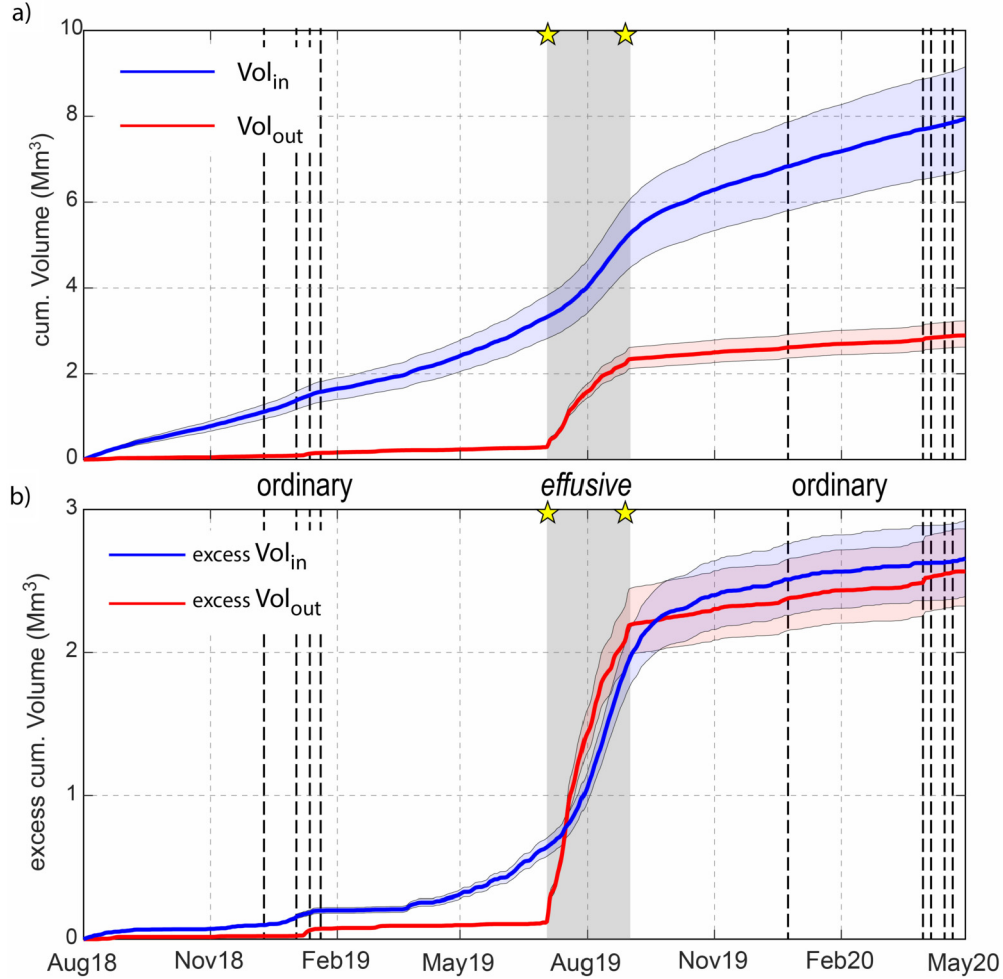
Fig. 6. (a) Cumulative magma input (Vol$_{in}$) and output volumes (Vol$_{out}$) associated with the Stromboli's shallow plumbing system during the 2019 eruption, with shaded fields representing the 25-75% confidence error bounds due to the conversion from experimental measurements on SO$_2$ fluxes and Volcanic Radiative Power; (b) excess input and output magma volumes obtained by detrending from both curves the average trend measured during the ordinary activity (see text for details). See Fig. 2 for other symbols.

in the descending magma flux Q_D, relative to its equilibrium state $Q_D{}^{ORD}$ during ordinary activity:

$$\Delta Q_D = Q_D - Q_D^{ORD} \qquad (4)$$

must produce a transient modification in the volume of the resident magma, and ultimately a transient pressure change within the conduit and/or shallow reservoir.

For such transient changes in the magma flow dynamics, we can approximate the volcanic system as behaving as a closed system, therefore expanding or contracting in response to any change in the resident magma volume. In this assumption, we can estimate the pressure change (ΔP) from the change in volume (ΔV) using: $\Delta P = \Delta V / (V * \beta)$ where β is the magma compressibility of the system and $\Delta V/V$ is the change in volume relative to the total volume of the shallow (HP) magma reservoir (V). Then, considering that $\Delta Q_D = \Delta V / \Delta t$, we can quantify the rate of pressure change $\Delta P/\Delta t$ from the observed magma flux perturbations ΔQ_D (excess descending magma flux) in the shallow magma feeding system (Fig. 7):

$$\frac{\Delta P}{\Delta t} = \frac{\Delta Q_D}{\beta V} \qquad (5)$$

where V is the total volume of the shallow (HP) magma reservoir, β is magma compressibility, and ΔQ_D is the excess de-

scending magma flux (Fig. 7). Considering a magma compressibility β of 1 to 5*10^{-9} Pa^{-1} (Cigolini et al., 2015) for the shallow (<3 km) HP magma, and a HP magma feeding system volume of 20-90 Mm^3 (Bragagni et al., 2014), we estimate the maximum pressure changes induced by transient variations in the excess descending magma flux (Fig. 7).

The relative ΔQ_D (Eq. (4)) and ΔP (Eq. (5)) changes allow defining four distinct volcanic activity phases. The ordinary phase preceding the eruption (*Phase I* in Fig. 8) is characterized by $\Delta Q_D \sim \Delta P / \Delta T \sim 0$ (Fig. 7) and Q$_{out}$ << Q$_{in}$ (Figs. 4–6). On July 3, 2019 the onset of the effusive activity (*Phase II* in Fig. 8) marks an abrupt Q$_D$ decrease, indicating more magma is being discharged than supplied (Q$_{out}$ > Q$_{in}$). This phase, lasting for ~40 days and corresponding to decompression rates of 1-30 Pas^{-1} (Fig. 8), is interpreted as caused by rapid drainage of upper conduit resident magma (Q$_{out}$ > Q$_{in}$; Fig. 4), ultimately leading to a cumulative decompression of ~10 MPa. Early in August 2019 (*Phase III* in Fig. 8), the Q$_D$ and ΔP trends exhibit an inversion from negative to positive values (Fig. 7), indicating onset of a new magma recharge phase (Q$_{in}$ > Q$_{out}$; Figs. 4–6) characterized by restored vigorous magma convective circulation in the conduit. The strong similarities between erupted and degassed magma volume estimates (Fig. 6) suggest that *Phase III* occurred in response to the rapid decompression *in Phase II*, e.g. that upward migration of deeper magma occurred to re-establish the equilibrium conduit condi-
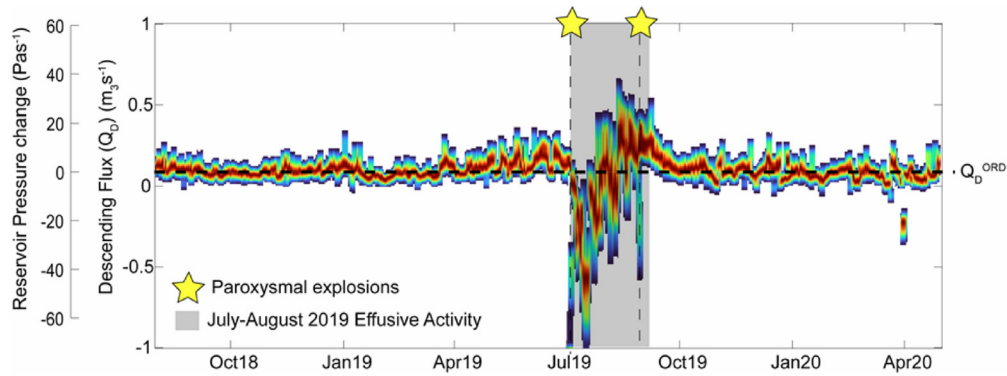
Fig. 7. Descending magma fluxes (Q_D) associated with the ordinary and eruptive dynamics of the Stromboli's shallow plumbing system, as derived by the difference between the daily averaged input and output magma fluxes. Black dotted line shows the Q_D value in ordinary activity (Q_D^{ORD}). Dark red colors correspond to 25-75% confidence interval derived from uncertainty estimate (see Fig. S1).

tions that were disrupted by rapid conduit emptying in *Phase II*. This phase culminated into the August 28 paroxysm. Finally, after the August 28 paroxysm (*Phase IV*; Fig. 8), the excess magma flux (ΔQ_D) decreases and magma input rate (Fig. 4) and SO_2 flux (Fig. 2) return in early October back to the pre-eruptive trend. This phase thus corresponds to magma input rate returning to the ordinary level of ~ 0.1 m^3/s (cf. Fig. 4), and an overall re-establishment of the pre-eruptive dynamical equilibrium conditions with ΔQ_D and ΔP (Fig. 7) close to 0. In summary, our results see the summer 2019 sequence as phases of discharge (*Phase II*)/recharge (*Phase III*) of the shallow Stromboli's feeding system, temporarily interrupting the ordinary convective magma circulation regime during ordinary activity (*Phases I and IV*).

Our results indicate that the effusive eruption is associated with an average daily decompression rate of up to 30 Pa/s (Fig. 7), and with a cumulative decompression ΔP of ~ 10 MPa in July 2019. This estimated pressure change is easily reconciled with the absence of measured deformation at surface during the eruption: assuming an open-conduit model, we infer that the observed pressure changes (Fig. 7) would have resulted into ground deformation rates (~ 0.01 - 0.1 μrad/day) and cumulative deformations (of 1-10 μrad for the entire eruption) well below those detectable by tiltmeters, and within their non-volcanic thermo-elastic noise (Bonaccorso et al., 2009). We additionally argue that the high magma compressibility, primarily determined by the exsolved volatiles in the magma (Huppert and Woods, 2002), may also contribute to explain the apparent discrepancy between the relatively large volume change in the conduit and the lack of significant

ground displacements at the surface (McCormick Kilbride et al., 2016; Mattia et al., 2021).

5.2. Implications for paroxysmal activity at Stromboli and for open-vent volcanoes

Our study, although admittedly having the 2019 effusive eruption as its primary target, also contributes to the debate on the dynamics and mechanisms driving the Stromboli's paroxysmal explosions (Aiuppa et al., 2021; Calvari et al., 2011; Ripepe et al., 2017, 2021; Andronico et al., 2021; Giudicepietro et al., 2020; Métrich et al., 2021; Viccaro et al., 2021). Petrologic evidence indicates that the gas-rich magma erupted during Stromboli's paroxysms is sourced by rapid magma transport from the deep (7-10 km) LP reservoir (Francalanci et al., 1999; Métrich et al., 2021). These models for a deep source of the paroxysms are consistent with gas (Aiuppa et al., 2021) and ground deformation (Ripepe et al., 2021) data, but have recently been challenged by observations/models that point to a shallow trigger (<1000 m deep) and/or put the accent on failure of the uppermost highly-viscous magma cap (Mattia et al., 2021; Viccaro et al., 2021). To add complexity, two recent paroxysms in 2003 and 2007 occurred during ongoing effusive activity, suggesting a causal mechanism between lava outpouring and paroxysms. Calvari et al. (2011), in particular, argued that paroxysms may be the ultimate result of decompression of the deep plumbing system, driven by emptying of the upper part of the magmatic conduit, especially in case of high lava discharge rate (Valade et al., 2016; Ripepe et al., 2017). Bottom-up (ascent of
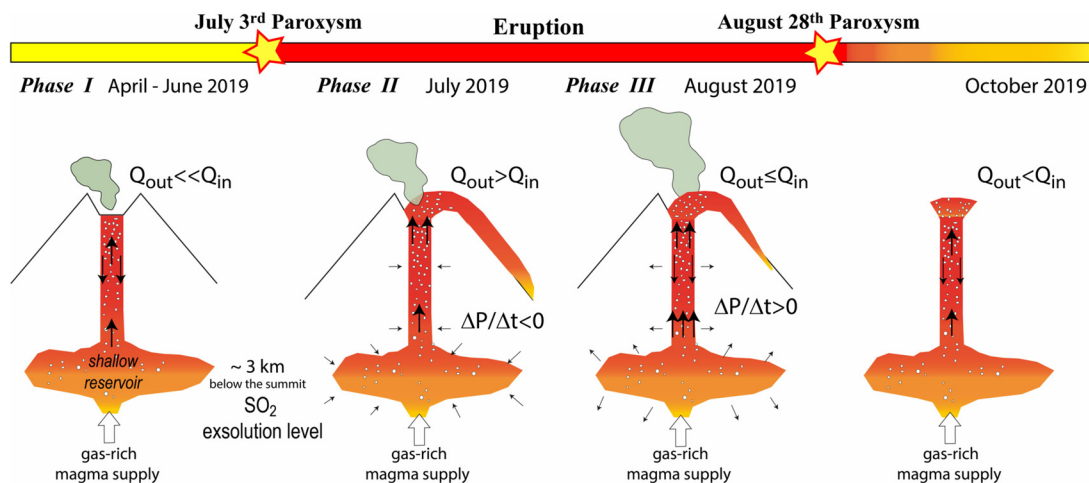

Fig. 8. Conceptual model of the shallow conduit dynamic before (*Phase I*), during (*Phase II and III*) and after (*Phase IV*) the 2019 eruption (see text for details).

gas-rich magma) and top-down (effusion-driven) mechanisms can also coexist within the same unrest, as indicated by the contrasting source processes suggested for the July 3, and the August 28, 2019 explosions (Aiuppa et al., 2021).

Our observations suggest that the July 3 paroxysm occurred when thermal and degassing activity were at the low to moderate levels (Fig. 2). However, we observe a mild SO_2 flux increase since May 2019 (Fig. 2) that, if combined with independent geophysical and volcanological observations (Andronico et al., 2021; Giudicepietro et al., 2020; Mattia et al., 2021; Viccaro et al., 2021), may be interpreted as evidence of escalating magma transport (Figs. 4, 6) in the shallow magmatic system starting about one month prior to the July 3. Gas observations (Aiuppa et al., 2021) indicate that the July 3 event was preceded by a precursory release of CO_2-rich bubbles sourced by later erupted LP magma; fluxing by deeply rising CO_2-rich bubbles may have therefore caused the accelerating shallow magma circulation (Fig. 4), SO_2 degassing (Fig. 2) and rate of ordinary explosions (Andronico et al., 2021) prior to July 3. We yet observe that this SO_2 flux increase is very mild, and that similar increases have frequently been observed during ordinary activity periods without having been followed by any paroxysm. This, and the fact that far more intense SO_2 flux variations, furthermore accompanied by persistent moderate to high thermal detections, have been observed prior to onset of effusive eruptions (Delle Donne et al., 2017; Valade et al., 2016), cast doubt on the "precursory" nature of this May 2019 SO_2 flux variation - that, as other supposed volcanological/geophysical precursors (Andronico et al., 2021; Giudicepietro et al., 2020), was only identified after post-hoc data analysis and re-processing. One important aspect, however, is that we find no evidence in our SO_2 flux record of a reduced gas output prior to the July 3 event. Therefore, our observations point against models invoking a role played by rheological stiffening and reduced permeability of the upper conduit magma as trigger for the blast (Mattia et al., 2021; Viccaro et al., 2021), and rather suggest rapid ascent of deep gas-rich magma and/or gas (Métrich et al., 2021; Aiuppa et al., 2021) as a more likely trigger.

The August 28 paroxysm occurred during the effusive crisis, when SO_2 and heat flux were both high (Figs. 4–7). In this case, as discussed previously in Aiuppa et al. (2021), our observations are consistent with the top-down mechanism, in which de-compressional, fast ascent and degassing of deep magma may have occurred in response to a rapid drainage of resident conduit magma into the lava flow field. The decompression rates calculated here for the 2019 eruption overlap with those estimated for recent paroxysms occurred in 2003 and 2007, for which the drainage of shallow magma during effusive activity has been considered as the trigger for LP, volatile-rich magma rise from depth (Aiuppa et al., 2021; Ripepe et al., 2017).

6. Conclusions

Our space- and ground-based measurements have allowed to shed light into conduit magma regime prior, during and after the 2019 Stromboli's effusive eruption. We show how thermal and SO_2 flux can be used to calculate the magma input and output rate. Our results confirm the large and well-known unbalance between magma input and output rates into the shallow (<3 km deep) feeding system during ordinary Strombolian activity, which is explained in terms of a convective regime. We demonstrate, for the first time, that this ordinary convecting magma regime was temporarily interrupted during the 2019 effusive phase, during which the output magma rate balanced, or even exceed for the first two weeks of the eruption, the magma input rate. We interpret our data in view of a discharge/recharge mechanism of the shallow plumbing system feeding surface activity; the partial failure of the SW crater outer rim during the July 3 paroxysm caused rapid emp-

tying of the shallow upper conduits ($\sim$50 m) leading to magma drainage into a rapidly developing lava flow field (*Phase II*). This event caused a $\sim$10 MPa decompression of the shallow plumbing system, which ultimately caused (in the ensuing *Phase III*) the ascent of new magma in the conduit to totally replace the $\sim$2 Mm^3 of magma erupted. This new conduit recharge phase may have been implicated as causal factor in forcing deep magma ascent during the August 28 paroxysm. Finally, besides the complexity of linking erupted and supplied magma volumes with continuous reliable estimates, our results also point out how these parameters, if well constrained, may allow to define changes in magma dynamics and ultimately in eruptive styles at active volcanoes.

CRediT authorship contribution statement

M.L., **D.D.D.** conceive the manuscript. **M.L.**, **D.D.D.**, **A.A.** and **M.R.** wrote the manuscript and realized the figures. **M.L.**, **D.C.** and **F.M.** analyzed the MODIS data. **D.D.D.**, **M.B.** and **F.P.L.** analyzed the UV-camera data. All the Authors have contributed to the acquisition, storage and processing of the presented datasets. **A.A.**, **D.C.**, **M.P.** and **M.R.** contributed to define the rationale and the method presented in the manuscript and supervised the manuscript. All the Authors provided information and/or critical comments during manuscript preparation.

Declaration of competing interest

The authors declare that they have no known competing financial interests or personal relationships that could have appeared to influence the work reported in this paper.

Data availability

All data generated or analyzed during this study are included in this published article (and its Supplementary Materials) or available by contacting the corresponding author upon reasonable request.

Appendix A. Supplementary material

Supplementary material related to this article can be found online at https://doi.org/10.1016/j.epsl.2022.117726.

References

Aiuppa, A., de Moor, J.M., Arellano, S., Coppola, D., Francofonte, V., Galle, B., Giudice, G., Liuzzo, M., Mendoza, E., Saballos, A., Tamburello, G., Battaglia, A., Bitetto, M., Gurrieri, S., Laiolo, M., Mastrolia, A., Moretti, R., 2018. Tracking formation of a lava lake from ground and space: Masaya volcano (Nicaragua), 2014–2017. Geochem. Geophys. Geosyst. 19, 496–515. https://doi.org/10.1002/2017GC007227.

Aiuppa, A., Bitetto, M., Delle Donne, D., La Monica, F., Tamburello, G., Coppola, D., Della Schiava, M., Innocenti, L., Lacanna, G., Laiolo, M., Massimetti, F., Pistolesi, M., Silengo, C., Ripepe, M., 2021. Volcanic CO_2 tracks the incubation period of basaltic paroxysms. Sci. Adv. 17 (7(38)). https://doi.org/10.1126/sciadv.abh0191.

Allard, P., Carbonnelle, J., Métrich, N., Loyer, H., Zettwoog, P., 1994. Sulphur output and magma degassing budget of Stromboli volcano. Nature 368, 326–330. https://doi.org/10.1038/368326a0.

Andronico, D., Del Bello, E., D'Oriano, C., Landi, P., Pardini, F., Scarlato, P., de' Michieli Vitturi, M., Taddeucci, J., Cristaldi, A., Ciancitto, F., Pennacchia, F., Ricci, T., Valentini, F., 2021. Uncovering the eruptive patterns of the 2019 double paroxysm eruption crisis of Stromboli volcano. Nat. Commun. 12, 4213. https://doi.org/10.1038/s41467-021-24420-1.

Bonaccorso, A., Bonforte, A., Gambino, S., Mattia, M., Guglielmino, F., Puglisi, G., Boschi, E., 2009. Insight on recent Stromboli eruption inferred from terrestrial and satellite ground deformation measurements. J. Volcanol. Geotherm. Res. 182 (3–4), 172–181. https://doi.org/10.1016/j.jvolgeores.2009.01.007.

Boudoire, G., Calabrese, S., Colacicco, A., Sordini, P., Habakaramo Macumu, P., Rafflin, V., Valade, S., Mweze, T., Kazadi Mwepu, J.C., Safari Habari, F., Amani Kahamire, T., Mumbere Mutima, Y., Ngaruye, J.C., Tuyishime, A., Tumaini Sadiki, A., Mavonga Tuluka, G., Mapendano Yalire, M., Kets, E.D., Grassa, F., D'Alessandro, W., Caliro, S., Rufino, F., Tedesco, D., 2022. Scientific response to the 2021 eruption of Nyiragongo based on the implementation of a participatory monitoring system. Sci. Rep. 12, 7488. https://doi.org/10.1038/s41598-022-11149-0.

Bragagni, A., Avanzinelli, R., Freymuth, H., Francalanci, L., 2014. Recycling of crystal mush-derived melts and short magma residence times revealed by U-series disequilibria at Stromboli. Earth Planet. Sci. Lett. 404, 206–219. https://doi.org/10.1016/j.epsl.2014.07.028.

Burton, M.R., Caltabiano, T., Murè, F., Salerno, G., Randazzo, D., 2009. SO_2 flux from Stromboli during the 2007 eruption: results from the FLAME network and traverse measurements. J. Volcanol. Geotherm. Res. 182 (3–4), 214–220. https://doi.org/10.1016/j.jvolgeores.2008.11.025.

Calvari, S., Spampinato, L., Bonaccorso, A., Oppenheimer, C., Rivalta, E., Boschi, E., 2011. Lava effusion—a slow fuse for paroxysms at Stromboli volcano? Earth Planet. Sci. Lett. 301, 317–323. https://doi.org/10.1016/j.epsl.2010.11.015.

Cigolini, C., Laiolo, M., Coppola, D., 2015. Revisiting the last major eruptions at Stromboli volcano: inferences on the role of volatiles during magma storage and decompression. In: Zellmer, G.F., Edmonds, M., Straub, S.M. (Eds.), The Role of Volatiles in the Genesis, Evolution and Eruption of Arc Magmas. In: Geological Society, London, Special Publications, vol. 410, pp. 143–177.

Coppola, D., Laiolo, M., Piscopo, D., Cigolini, C., 2013. Rheological control on the radiant density of active lava flows and domes. J. Volcanol. Geotherm. Res. 249, 39–48. https://doi.org/10.1016/j.jvolgeores.2012.09.005.

Coppola, D., Laiolo, M., Cigolini, C., Delle Donne, D., Ripepe, M., 2016. Enhanced volcanic hot-spot detection using MODIS IR data: results from the MIROVA system. In: Harris, A.J.L., De Groeve, T., Garel, F., Carn, S.A. (Eds.), Detecting, Modelling, and Responding to Effusive Eruptions. In: Geological Society, London, Special Publications.

Coppola, D., Laiolo, M., Massimetti, F., Cigolini, C., 2019. Monitoring endogenous growth of open-vent volcanoes by balancing thermal and SO_2 emissions data derived from space. Sci. Rep. 9, 9394. https://doi.org/10.1038/s41598-019-45753-4.

D'Aleo, R., Bitetto, M., Delle Donne, D., Coltelli, M., Coppola, D., McCormick Kilbride, B., Pecora, E., Ripepe, M., Salem, L.C., Tamburello, G., Aiuppa, A., 2018. Understanding the SO2 degassing budget of Mt Etna's Paroxysms: first clues from the December 2015 sequence. Front. Earth Sci. 14. https://doi.org/10.3389/feart.2018.00239.

Delle Donne, D., Tamburello, G., Aiuppa, A., Bitetto, M., Lacanna, G., D'Aleo, R., Ripepe, M., 2017. Exploring the explosive-effusive transition using permanent ultra-violet cameras. J. Geophys. Res., Solid Earth 122, 4377–4394. https://doi.org/10.1002/2017JB014027.

Devine, J.D., Sigurdsson, H., Davis, A.N., Self, S., 1984. Estimates of sulfur and chlorine yield to the atmosphere from volcanic eruptions and potential climatic effects. J. Geophys. Res. 89, 6309–6325. https://doi.org/10.1029/JB089iB07p06309.

Di Stefano, F., Mollo, S., Ubide, T., Petrone, C.M., Caulfield, J., Scarlato, P., Nazzari, M., Andronico, D., Del Bello, E., 2020. Mush cannibalism and disruption recorded by clinopyroxene phenocrysts at Stromboli volcano: new insights from recent 2003-2017 activity. Lithos 360–361, 105440. https://doi.org/10.1016/j.lithos.2020.105440.

Di Traglia, F., Fornaciai, A., Casalbore, D., Favalli, M., Manzella, I., Romagnoli, C., Chiocci, F.L., Cole, P., Nolesini, T., Casagli, N., 2021a. Subaerial-submarine morphological changes at Stromboli volcano (Italy) induced by the 2019–2020 eruptive activity. Geomorphology 400, 108093. https://doi.org/10.1016/j.geomorph.2021.

Di Traglia, F., De Luca, C., Manzo, M., Nolesini, T., Casagli, N., Lanari, R., Casu, F., 2021b. Joint exploitation of space-borne and ground-based multitemporal InSAR measurements for volcano monitoring: the Stromboli volcano case study. Remote Sens. Environ. 260, 112441. https://doi.org/10.1016/j.rse.2021.112441.

Edmonds, M., Liu, E., Cashman, K.V., 2022. Open-vent volcanoes fuelled by depth-integrated magma degassing. Bull. Volcanol. 84 (3). https://doi.org/10.1007/s00445-021-01522-8.

Francalanci, L., Tommasini, S., Conticelli, S., Davies, G.R., 1999. Sr isotope evidence for short magma residence time for the 20th century activity at Stromboli volcano, Italy. Earth Planet. Sci. Lett. 167 (1–2), 61–69. https://doi.org/10.1016/S0012-821X(99)00013-8.

Francis, P., Oppenheimer, C., Stevenson, D., 1993. Endogenous growth of persistently active volcanoes. Nature 366, 554–557. https://doi.org/10.1038/366554a0.

Giordano, G., De Astis, G., 2021. The summer 2019 basaltic Vulcanian eruptions (paroxysms) of Stromboli. Bull. Volcanol. 83. https://doi.org/10.1007/s00445-020-01423-2.

Giudicepietro, F., López, C., Macedonio, G., Alparone, S., Bianco, F., Calvari, S., De Cesare, W., Delle Donne, D., Di Lieto, B., Esposito, A.M., Orazi, M., Peluso, R., Privitera, E., Romano, P., Scarpato, G., Tramelli, A., 2020. Geophysical precursors of the July-August 2019 paroxysmal eruptive phase and their implications for Stromboli volcano (Italy) monitoring. Sci. Rep. 10, 10296. https://doi.org/10.1038/s41598-020-67220-1.

Harris, A.J.L., Stevenson, D.S., 1997. Magma budgets and steady-state activity of Vulcano and Stromboli volcanoes. Geophys. Res. Lett. 24, 1043–1046. https://doi.org/10.1029/97GL00861.

Huppert, H.E., Woods, A.W., 2002. The role of volatiles in magma chamber dynamics. Nature 420, 493–495. https://doi.org/10.1038/nature01211.

Kazahira, K., Shinohara, H., Saito, G., 1994. Excessive degassing of izu-Oshima volcano: magma convection in a conduit. Bull. Volcanol. 56, 207–216. https://doi.org/10.1007/BF00279605.

Kern, C., Lerner, A.H., Elias, T., Nadeau, P.A., Holland, L., Kelly, P.J., Werner, C.A., Clor, L.E., Cappos, M., 2020. Quantifying gas emissions associated with the 2018 rift eruption of Kīlauea volcano using ground-based DOAS measurements. Bull. Volcanol. 82, 55. https://doi.org/10.1007/s00445-020-01390-8.

Lacanna, G., Ripepe, M., 2020. Genesis of tsunami waves generated by pyroclastic flows and the early-warning system. In: Abstract Volume 4a, Conferenza A. Rittmann, Catania.

Laiolo, M., Massimetti, F., Cigolini, C., Ripepe, M., Coppola, D., 2018. Long-term eruptive trends from space-based thermal and emissions: a comparative analysis of Stromboli, Batu Tara and Tinakula volcanoes. Bull. Volcanol. 80 (9). https://doi.org/10.1007/s00445-018-1242-0.

Mattia, M., Di Lieto, B., Ganci, G., Bruno, V., Romano, P., Ciancitto, F., De Martino, P., Gambino, S., Aloisi, M., Sciotto, M., Scarpa, R., Ferlito, C., 2021. The 2019 eruptive activity at Stromboli volcano: a multidisciplinary approach to reveal hidden features of the "unexpected" 3 July Paroxysm. Remote Sens. 13, 4064. https://doi.org/10.3390/rs13204064.

McCormick Kilbride, B., Edmonds, M., Biggs, J., 2016. Observing eruptions of gas-rich compressible magmas from space. Nat. Commun. 7, 13744. https://doi.org/10.1038/ncomms13744.

Métrich, N., Bertagnini, A., Di Muro, A., 2010. Conditions of magma storage, degassing and ascent at Stromboli: new insights into the volcano plumbing system with inferences on the eruptive dynamics. J. Petrol. 51, 603–626. https://doi.org/10.1093/petrology/egp083.

Métrich, N., Bertagnini, A., Pistolesi, M., 2021. Paroxysms at Stromboli volcano (Italy): source, genesis and dynamics. Front. Earth Sci. 9, 593339. https://doi.org/10.3389/feart.2021.593339.

Oppenheimer, C., Scaillet, B., Woods, A., Sutton, J.A., Elias, T., Moussallam, Y., 2018. Influence of eruptive style on volcanic gas emission chemistry and temperature. Nat. Geosci. 11, 678–681. https://doi.org/10.1038/s41561-018-0194-5.

Petrone, C.M., Braschi, E., Francalanci, L., Casalini, M., Tommasini, S., 2018. Rapid mixing and short storage timescale in the magma dynamics of a steady-state volcano. Earth Planet. Sci. Lett. 492, 206–221. https://doi.org/10.1016/j.epsl.2018.03.055.

Phillipson, G., Sobradelo, R., Gottsmann, J., 2013. Global volcanic unrest in the 21st century: an analysis of the first decade. J. Volcanol. Geotherm. Res. 264, 183–196. https://doi.org/10.1016/j.jvolgeores.2013.08.004.

Plank, S., Marchese, F., Filizzola, C., Pergola, N., Neri, M., Nolde, M., Martinis, S., 2019. The July/August 2019 lava flows at the Sciara del Fuoco, Stromboli–analysis from multi-sensor infrared satellite imagery. Remote Sens. 11 (23), 2879. https://doi.org/10.3390/rs11232879.

Ripepe, M., Marchetti, E., Ulivieri, G., Harris, A.J.L., Dehn, J., Burton, M., Caltabiano, T., Salerno, G., 2005. Effusive to explosive transition during the 2003 eruption of Stromboli volcano. Geology 33, 341–344. https://doi.org/10.1130/G21173.1.

Ripepe, M., Delle Donne, D., Harris, A.J.L., Marchetti, E., Ulivieri, G., 2008. Dynamics of Strombolian activity. In: Calvari, S., Inguaggiato, S., Puglisi, G., Ripepe, M., Rosi, M. (Eds.), Learning from Stromboli: An Integrated Study of the 2002-2003 Eruption. In: AGU Geophysics Monograph Series, vol. 182, pp. 39–48.

Ripepe, M., Delle Donne, D., Genco, R., Maggio, G., Pistolesi, M., Marchetti, E., Lacanna, G., Ulivieri, G., Poggi, P., 2015. Volcano seismicity and ground deformation unveil the gravity-driven magma discharge dynamics of a volcanic eruption. Nat. Commun. 6, 6998. https://doi.org/10.1038/ncomms7998.

Ripepe, M., Pistolesi, M., Coppola, D., Delle Donne, D., Genco, R., Lacanna, G., Laiolo, M., Marchetti, E., Ulivieri, G., Valade, S., 2017. Forecasting effusive dynamics and decompression rates by magmastatic model at open-vent volcanoes. Sci. Rep. 7, 3885. https://doi.org/10.1038/s41598-017-03833-3.

Ripepe, M., Lacanna, G., Pistolesi, M., Silengo, M.C., Aiuppa, A., Laiolo, M., Massimetti, F., Innocenti, L., Della Schiava, M., Bitetto, M., La Monica, F.P., Nishimura, T., Rosi, M., Mangione, D., Ricciardi, A., Genco, R., Coppola, D., Marchetti, E., Delle Donne, D., 2021. Ground deformation reveals the scale-invariant conduit dynamics driving explosive basaltic eruptions. Nat. Commun. 12, 1683. https://doi.org/10.1038/s41467-021-21722-2.

Rose, W.I., Palma, J.L., Delgado Granados, H., Varley, N., 2013. Open-vent volcanism and related hazards: overview. Spec. Pap., Geol. Soc. Am. 498, vii–xiii. https://doi.org/10.1130/2013.2498(00).

Rosi, M., Pistolesi, M., Bertagnini, A., Landi, P., Pompilio, M., Di Roberto, A., 2013. Stromboli volcano, Aeolian Islands (Italy): present eruptive activity and hazards. Mem. Geol. Soc. Lond. 37, 473–490. https://doi.org/10.1144/M37.14. Ch. 14.

Shinohara, H., 2008. Excess degassing from volcanoes and its role on eruptive and intrusive activity. Rev. Geophys. 46. https://doi.org/10.1029/2007RG000244.

Shreve, T., Grandin, R., Boichu, M., Garaebiti, E., Moussallam, Y., Ballu, V., Delgado, F., Leclerc, F., Vallée, M., Henriot, N., Cevuard, S., Tari, D., Lebellegard, P., Pelletier, B., 2019. From prodigious volcanic degassing to caldera subsidence and quiescence at Ambrym (Vanuatu): the influence of regional tectonics. Sci. Rep. 9, 18868. https://doi.org/10.1038/s41598-019-55141-7.

Stevenson, D.S., Blake, S., 1998. Modelling the dynamics and thermodynamics of volcanic degassing. Bull. Volcanol. 60, 307–317. https://doi.org/10.1007/s004450050234.

Valade, S., Lacanna, G., Coppola, D., Laiolo, M., Pistolesi, M., Delle Donne, D., Genco, R., Marchetti, E., Ulivieri, G., Allocca, C., Cigolini, C., Nishimura, T., Poggi, P., Ripepe, M., 2016. Tracking dynamics of magma migration in open-conduit systems. Bull. Volcanol. 78, 11. https://doi.org/10.1007/s00445-016-1072-x.

Viccaro, M., Cannata, A., Cannavò, F., De Rosa, R., Giuffrida, M., Nicotra, E., Petrelli, M., Sacco, G., 2021. Shallow conduit dynamics fuel the unexpected paroxysms of Stromboli volcano during the summer 2019. Sci. Rep. 11, 266. https://doi.org/10.1038/s41598-020-79558-7.

Web References

LGS Report. http://lgs.geo.unifi.it/index.php/reports/stromboli-daily; http://lgs.geo.unifi.it/index.php/reports/stromboli-weekly, 2022. (Accessed 9 March 2022).

INGV Report. https://www.ct.ingv.it/index.php/monitoraggio-e-sorveglianza/prodotti-del-monitoraggio/bollettini-settimanali-multidisciplinari. (Accessed 9 March 2022).